

Nodeless superconductivity in kagome metal CsV_3Sb_5 with and without time reversal symmetry breaking

Wei Zhang,¹ Xinyou Liu,¹ Lingfei Wang,¹ Chun Wai Tsang,¹ Zheyu Wang,¹ Siu Tung Lam,¹ Wenyan Wang,¹ Jianyu Xie,¹ Xuefeng Zhou,² Yusheng Zhao,² Shanmin Wang,² Jeff Tallon,³ Kwing To Lai*,^{1,4} and Swee K. Goh†¹

¹*Department of Physics, The Chinese University of Hong Kong, Shatin, Hong Kong, China*

²*Department of Physics, Southern University of Science and Technology, Shenzhen, Guangdong, China*

³*Robinson Institute, Victoria University of Wellington, P.O. Box 600, Wellington, New Zealand*

⁴*Shenzhen Research Institute, The Chinese University of Hong Kong, Shatin, Hong Kong, China*

(Dated: January 19, 2023)

The kagome metal CsV_3Sb_5 features an unusual competition between the charge-density-wave (CDW) order and superconductivity. Evidence for time-reversal symmetry breaking (TRSB) inside the CDW phase has been accumulating. Hence, the superconductivity in CsV_3Sb_5 emerges from a TRSB normal state, potentially resulting in an exotic superconducting state. To reveal the pairing symmetry, we first investigate the effect of nonmagnetic impurity. Our results show that the superconducting critical temperature is insensitive to disorder, pointing to conventional s -wave superconductivity. Moreover, our measurements of the self-field critical current ($I_{c,sf}$), which is related to the London penetration depth, also confirm conventional s -wave superconductivity with strong coupling. Finally, we measure $I_{c,sf}$ where the CDW order is removed by pressure and superconductivity emerges from the pristine normal state. Our results show that s -wave gap symmetry is retained, providing strong evidence for the presence of conventional s -wave superconductivity in CsV_3Sb_5 irrespective of the presence of the TRSB.

Keywords: Kagome metal CsV_3Sb_5 , superconducting gap, critical current, time reversal symmetry breaking

Kagome metals AV_3Sb_5 ($A=\text{K}, \text{Rb}, \text{Cs}$) have been heavily studied recently due to their exotic properties including non-trivial topology, anomalous Hall effect (AHE), and interesting interplay between superconductivity and unconventional charge density wave (CDW) [1–20]. Among the three compounds, CsV_3Sb_5 possesses the highest $T_c \sim 2.7$ K with a second-order CDW phase transition occurring at $T_{\text{CDW}} \sim 90$ K [1, 2]. From the zero-field muon spin relaxation (ZF- μSR) and magneto-optic polar Kerr effect measurements, evidence of time-reversal symmetry breaking (TRSB) has been detected in the CDW phase. Concurrently, anomalous Hall effect without local moments occurs [17, 19, 21, 22]. To explain the observed AHE and TRSB, a chiral flux phase (CFP) of CDW has been proposed [23]. Hence, the superconducting state in CsV_3Sb_5 emerges from a TRSB normal state, potentially resulting in an exotic superconducting ground state.

The pairing symmetry can shed light on the unconventional nature of the superconductivity. However, the pairing symmetry of CsV_3Sb_5 remains controversial based on existing experimental results. Scanning tunneling microscopy (STM) has detected a V-shape density of states, indicating a gapless superconductivity [6, 24, 25]. Furthermore, thermal conductivity shows a finite residual linear term in the 0 K limit, lending support to a nodal superconducting gap [26]. On the other hand, the magnetic penetration depth revealed by both tunnel diode oscillator (TDO) and muon spin rotation (μSR) experiments suggest nodeless superconductivity in CsV_3Sb_5 [27–31]. Moreover, from the spin-lattice relaxation measurement, a finite Hebel-Slichter coherence

peak is observed just below T_c , indicating a conventional s -wave pairing [32].

Whether or not TRSB has an influence on the pairing symmetry needs to be clarified urgently. One approach is to remove the CDW state completely, and investigate the pristine superconducting phase. This total suppression of the CDW phase can be achieved by applying a hydrostatic pressure greater than ~ 20 kbar [4, 19]. Thus, a careful examination of the superconducting ground state of CsV_3Sb_5 without the complication due to TRSB can be performed, and this forms the major theme of this manuscript. To accomplish this objective, a probe that can detect the superconducting gap under pressure is needed.

Recently, the superfluid density has been shown to be related to the self-field critical current density ($J_{c,sf}$), *i.e.* the transport critical current density in the absence of an external magnetic field [33–35]. Thus, by measuring the temperature dependence of the critical current, the gap symmetry and the coupling strength can be extracted. Measurement of $J_{c,sf}$ has been demonstrated under pressure [36, 37]. Therefore, the examination of $J_{c,sf}$ provides a novel route to probe the superconducting gap and superfluid density at any pressure.

Apart from the self-field critical current, the effect of nonmagnetic impurities can also give information on the superconducting gap symmetry. In s -wave superconductors without sign change of the gap, Anderson’s theorem dictates that Cooper pairs are not destroyed by nonmagnetic impurities and hence, T_c is more robust against the disorder level [38, 39]. However, if the gap is formed by portions with different signs or there are nodes in the

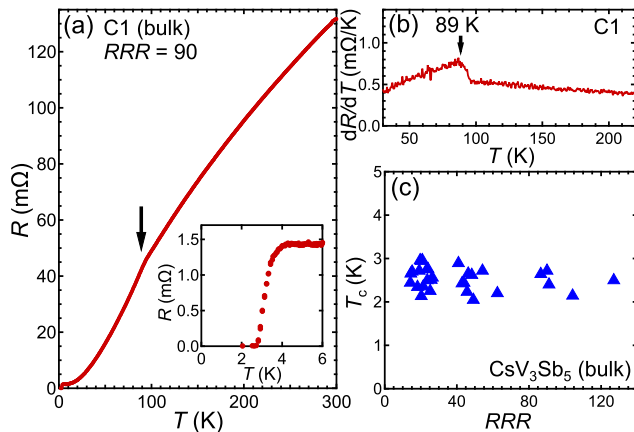


FIG. 1 (a) Temperature dependence of electrical resistance of the bulk CsV_3Sb_5 (sample C1) with a RRR of 90. The inset shows the superconducting transition. (b) Temperature dependence of dR/dT , displaying a sharp peak at T_{CDW} . (c) T_c of 30 bulk samples with different RRR values.

gap, such as an s_{\pm} state or a d -wave state, nonmagnetic impurities will be pair-breaking and suppress T_c rapidly [38–43].

In this article, we explore the nature of the superconducting gap in CsV_3Sb_5 with and without TRSB. At ambient pressure, where TRSB is present, we measure the T_c of a large number of crystals with varying residual resistivity ratios (RRRs). Scanning tunneling microscopy detected the presence of Cs/Sb vacancies or V defect [24, 44]. Therefore, the different RRR values could originate from different concentrations of vacancies and defect. Crucially, these are nonmagnetic impurities, providing the avenue to investigate their effect on T_c . Next, we probe the superconducting state by $J_{c,sf}$. The insensitivity of T_c to disorder and the T -dependence of $J_{c,sf}$ both indicate a conventional s -wave superconductivity. To investigate the role of the TRSB CDW phase on the superconductivity, we further detect the critical current under high pressures where the CDW phase is totally suppressed. The superconductivity which emerges from the pristine phase also follows the nodeless s -wave gap symmetry. Our results show that TRSB in the CDW phase does not modify the nodeless property of the superconducting gap.

Figure 1(a) shows the temperature dependence of the electrical resistance $R(T)$ for one of the single-crystalline CsV_3Sb_5 samples in bulk form. On cooling, $R(T)$ decreases and an anomaly appears at around 89 K. Correspondingly, a peak appears in dR/dT , as displayed in Fig. 1(b), which is consistent with the reported CDW transition. With further cooling, $R(T)$ shows the superconducting transition with $T_c \sim 2.8$ K (see the lower inset in Fig. 1(a)). We have taken the temperature at which the resistance reaches zero as T_c . The RRR (defined as $R(300 \text{ K})/R(5 \text{ K})$) is 90 for sample C1. Next, we study

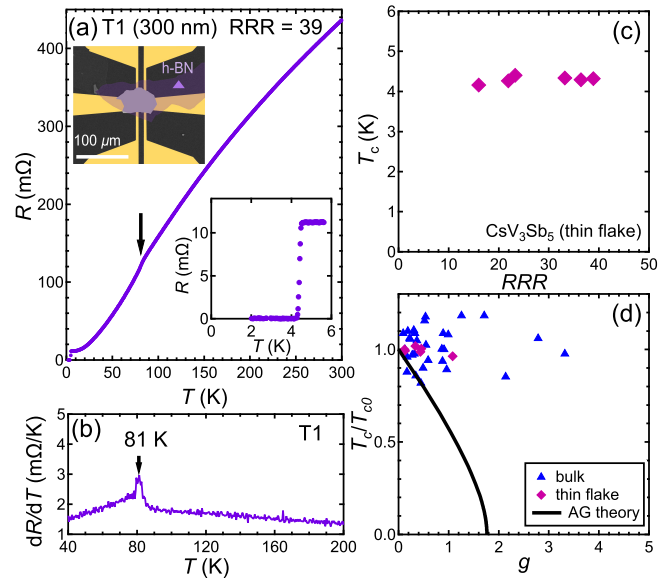


FIG. 2 (a) Temperature dependence of electrical resistance of a thin flake of CsV_3Sb_5 (T1). The upper inset is the scanning electron microscope (SEM) image of a CsV_3Sb_5 thin flake sitting on diamond anvil pre-patterned with electrodes. The sample is covered with h-BN. False colors are used for illustration. The lower inset shows the superconducting transition. (b) Temperature dependence of dR/dT , displaying a sharp peak at T_{CDW} . (c) T_c of thin flakes with various RRR values. (d) T_c of CsV_3Sb_5 as a function of the dimensionless scattering rate g . The solid line represents the suppression of T_c expected in the Abrikosov-Gor'kov (AG) theory.

30 CsV_3Sb_5 samples in bulk form (see Supporting Information S1 for additional $\rho - T$ curves). As shown in Fig. 1(c), although the RRR spans a large range from 14 to 127, T_c in CsV_3Sb_5 is clearly independent of the RRR values. Therefore, T_c is insensitive to disorder, suggesting the absence of nodes in the superconducting gap [40, 41]. We note that the RRR dependence of T_{CDW} is also weak (see Supporting Information S1).

We have also studied CsV_3Sb_5 in the form of thin flakes. As shown in the upper inset of Fig. 2(a), we conduct electrical transport measurements on the flake placed on a diamond substrate pre-patterned with electrodes. The diamond substrate provides an ideal platform to ensure that the flake is thermally anchored to the cold head. We have adopted a similar configuration to measure the Shubnikov-de Haas effect of thin CsV_3Sb_5 [45]. As we reported in Ref. [45], T_c is enhanced and the superconducting transition becomes sharper in the thin flake. The higher T_c may result from a possible orbital selective hole doping mechanism [45]. Here, we study six CsV_3Sb_5 thin flakes to investigate the RRR dependence (see Supporting Information S1 for more $\rho - T$ curves). As shown in Fig. 2(c), T_c is still independent of RRR and it is less scattered about the average value

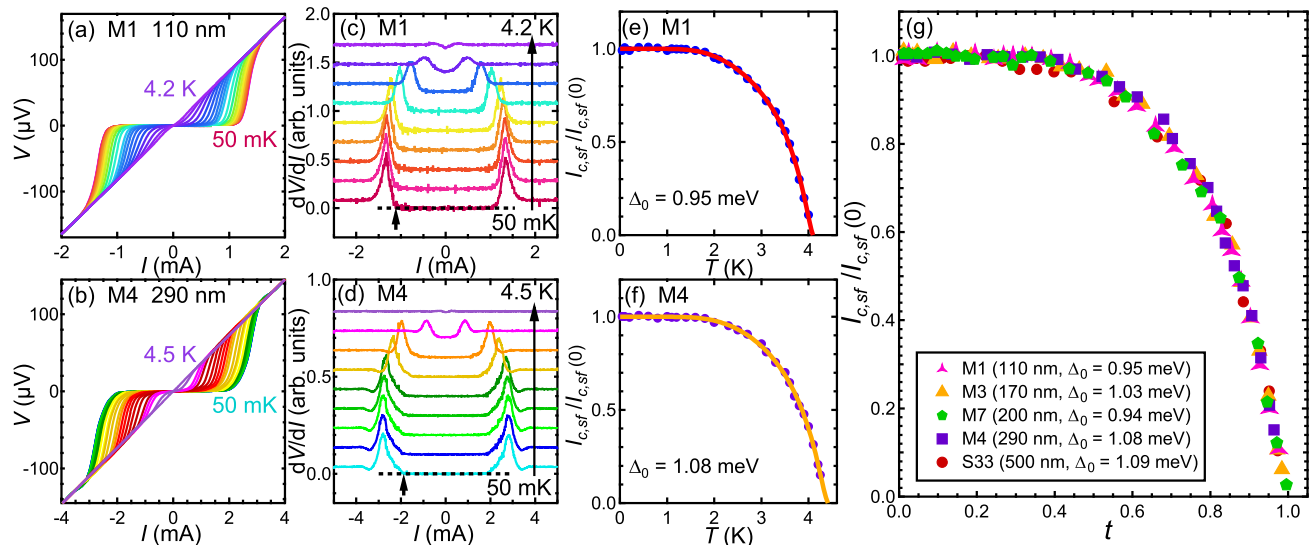


FIG. 3 V - I characteristics for thin flake (a) M1 (110 nm) and (b) M4 (290 nm). The calculated first derivative of $V(I)$, dV/dI , of (c) M1 and (d) M4. The short black arrows indicate the onset of deviation from $dV/dI = 0$, which we define as the critical current I_c . The long arrows show the direction of increasing temperature. Temperature dependence of critical current normalized by critical current at 0 K limit $I_{c,sf}(0)$ of (e) M1 and (f) M4. The solid curves are the single s -wave gap fits. (g) $I_{c,sf}(T)/I_{c,sf}(0)$ as a function of the reduced temperature $t = T/T_c$ for all measured thin flakes.

compared with the bulk counterpart. Note that to rule out possible influence of the thickness dependence, all the thin flake samples used in Fig. 2(c) are around 250 nm.

To quantify the rate at which T_c can be suppressed by impurities, we introduce a dimensionless scattering rate, defined as [46]

$$g = \frac{\hbar}{k_B \mu_0} \frac{\rho_0}{T_{c0} \lambda^2} \quad (1)$$

where μ_0 is the vacuum permeability, k_B is Boltzmann constant, ρ_0 is the residual resistivity and λ is the London penetration depth. In this study, we use the resistivity values at 5 K for ρ_0 for each sample and we take $\lambda = 450$ nm [27]. T_{c0} is the transition temperature in the clean limit. Hence, we take the T_c of the largest RRR sample as T_{c0} : $T_{c0} = 2.5$ K for the bulk sample and $T_{c0} = 4.3$ K for the thin flake. Figure 2(d) shows T_c/T_{c0} against g for all samples (symbols). Also shown on the figure is a theoretical curve based on Abrikosov-Gor'kov theory, which describes the suppression of T_c for a superconductor with a sign-changing gap when nonmagnetic impurities are introduced, or for a conventional s -wave superconductor in the presence of magnetic impurities. As can be seen in Fig. 2(d), T_c in CsV_3Sb_5 is not sensitive to disorder even though g has spanned a large range, unambiguously pointing to a conventional s -wave superconductivity scenario.

To corroborate the proposal of the nodeless superconductivity in CsV_3Sb_5 , we further conduct critical current measurements on the thin flakes of CsV_3Sb_5 .

Figures 3(a) and 3(b) show the voltage-current (V - I) curves at various temperatures in two representative thin flake samples M1 (thickness, $2b = 170$ nm) and M4 ($2b = 290$ nm). At a fixed temperature, a pulsed current is applied perpendicular to the cross-section of the thin flakes. For a typical trace, a drastic increase of the voltage is recorded when the current exceeds a threshold, indicating a recovery from the superconducting state to the normal state. We take the current when dV/dI first deviates from zero to be the critical current, see the short arrows in Figs. 3(c) and 3(d). Figures 3(e) and 3(f) show the temperature dependence of critical current normalized by critical current at 0 K limit, $I_{c,sf}(T)/I_{c,sf}(0)$, down to 50 mK. Since $I_{c,sf}(T)$ is essentially temperature-independent below ~ 1.5 K, we take $I_{c,sf}(50 \text{ mK})$ as $I_{c,sf}(0)$. The experimental data are shown as solid symbols. When the temperature is reduced, $I_{c,sf}(T)/I_{c,sf}(0)$ first increases significantly and then rapidly saturates at the zero temperature limit, which we will show to be consistent with a nodeless order parameter [33–35].

When the half-thickness (b) of the flake is smaller than the penetration depth (λ), the self-field critical current density ($J_{c,sf}$), i.e. the transport critical current density at the zero magnetic field, is recently established to relate to the penetration depth λ as follows [33]:

$$J_{c,sf} = \frac{\phi_0}{4\pi\mu_0\lambda^3} \left(\ln \frac{\lambda}{\xi} + 0.5 \right) \quad (2)$$

where ϕ_0 is the flux quantum and ξ is the coherence length. Since the superfluid density $\rho_s \propto \lambda^{-2}$, the tem-

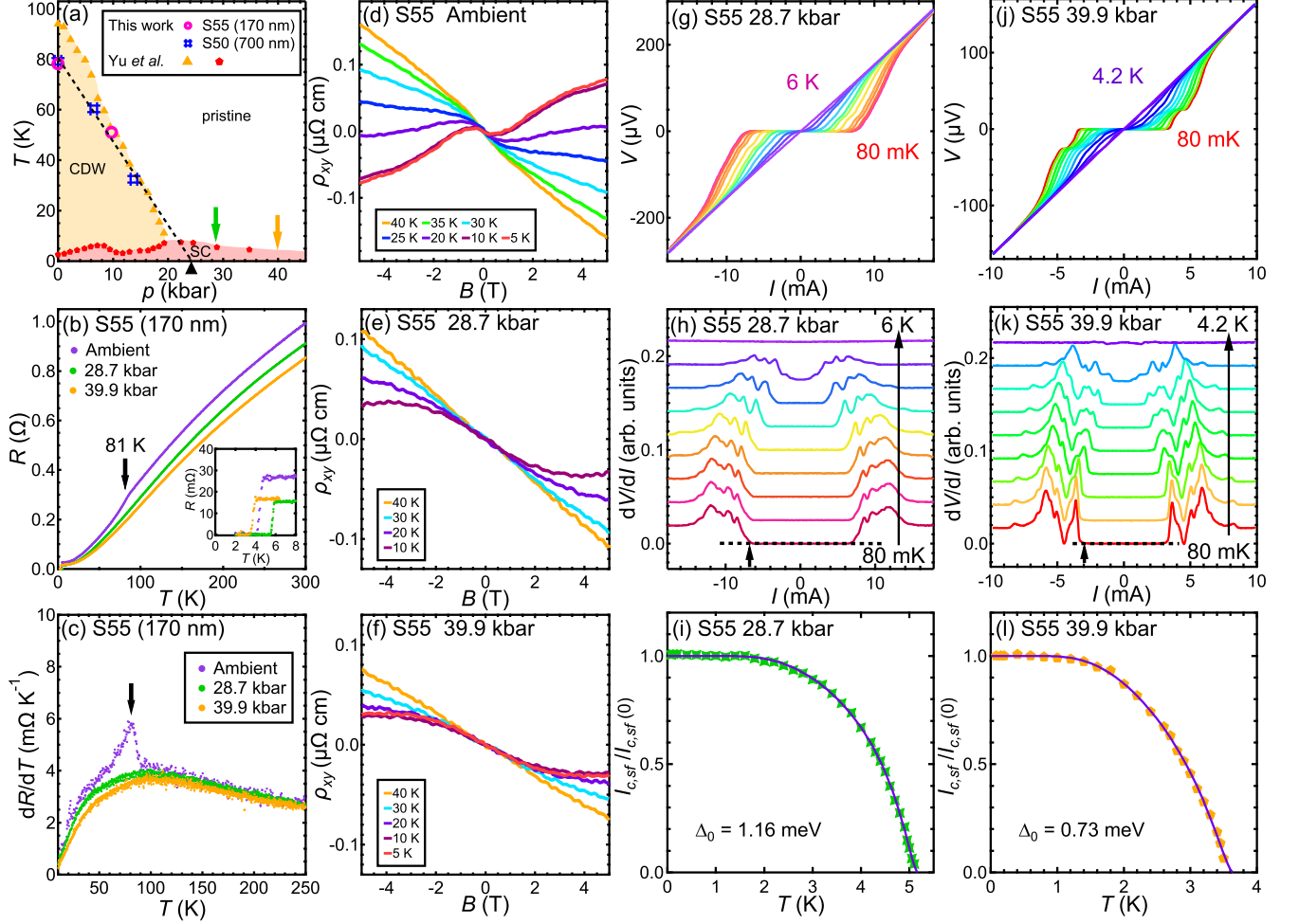


FIG. 4 (a) Temperature-pressure phase diagram of CsV_3Sb_5 . The solid symbols are adapted from Ref. [19], where the CDW phase is totally suppressed at around 20 kbar. The open symbols represent the T_{CDW} in thin flakes measured by us, where the CDW phase is suppressed at around 24 kbar based on linear extrapolation, as indicated by the up-triangle. The green and yellow arrows at 28.7 kbar and 39.9 kbar, respectively, indicate the pressure values chosen for investigating superconductivity free of TRSB. (b) Temperature dependence of resistance of S55 (170 nm) at ambient pressure, 28.7 kbar and 39.9 kbar. The inset shows the superconducting transition. (c) Temperature dependence of dR/dT of S55 at ambient pressure, 28.7 kbar and 39.9 kbar. The arrow indicates T_{CDW} . (d) Hall resistivity ρ_{xy} of S55 at different temperatures at (d) ambient pressure, (e) 28.7 kbar and (f) 39.9 kbar. V - I characteristics of S55 at different temperatures at (g) 28.7 kbar and (j) 39.9 kbar. The calculated first derivative of $V(I)$, dV/dI , of S55 at (h) 28.7 kbar and (k) 39.9 kbar. The short black arrows indicate the onset of deviation from $dV/dI = 0$, which we define as the critical current I_c . The long arrows show the direction of increasing temperature. Temperature dependence of $I_{c,sf}(T)/I_{c,sf}(0)$ of S55 at (i) 28.7 kbar and (l) 39.9 kbar. The solid curves are the single s -wave gap fits.

perature dependence of ρ_s can be determined by a careful measurement of $J_{c,sf}(T)$, allowing a discussion of the superconducting gap. In particular, for s -wave symmetry with a single gap,

$$\frac{\rho_s(T)}{\rho_s(0)} = \frac{\lambda(T)^{-2}}{\lambda(0)^{-2}} = 1 - 2\sqrt{\frac{\pi\Delta(0)}{k_B T}} e^{-\Delta(0)/k_B T}. \quad (3)$$

From the muon spin rotation measurement, the pen-

etration depth of CsV_3Sb_5 is around 450 nm in the low temperature limit [27]. Thus, Eqn. (2) is applicable to both M1 and M4 as both flakes satisfy the condition $b \ll \lambda$. In fact, $I_{c,sf}(T)/I_{c,sf}(0) = J_{c,sf}(T)/J_{c,sf}(0)$, because the sample geometry is temperature independent and the terms enclosed in the brackets in Eqn. (2) can be regarded as constants because of the logarithm. Thus, we can use the combination of Eqns. (2) and (3) to analyze

our data. As shown in Figs. 3(e) and 3(f), the experimental data can be accurately described by assuming an *s*-wave gap (solid curves). Besides, the extracted superconducting gap values are 0.95 meV ($2.70 k_B T_c$) and 1.08 meV ($2.84 k_B T_c$) for M1 and M4, respectively, which are larger than the BCS weak coupling limit ($1.76 k_B T_c$), indicating strong-coupling superconductivity. The strong coupling nature of the superconductivity revealed here is consistent with previous studies (see Supporting Information S3 for a comparison with the literature values). Figure 3(g) displays $I_{c,sf}(T)/I_{c,sf}(0)$ versus the reduced temperature $t = T/T_c$ for all thin flakes we study and all the datasets collapse into a single curve, indicating both the consistency of our results and the preservation of the same order parameter down to the lowest temperature.

To investigate the possible influence of TRSB – introduced via the CDW order – on the superconducting gap, we take advantage of the known temperature-pressure phase diagram constructed for CsV_3Sb_5 . For the bulk system, the CDW order can be completely suppressed by a pressure of ~ 20 kbar while in the thin flake, the CDW order disappears at ~ 24 kbar (Fig. 4(a)). Thus, we performed two experiments at 28.7 kbar and 39.9 kbar to examine the superconducting state without the complication due to TRSB. The absence of the CDW order at 28.7 kbar and 39.9 kbar is evidenced in $R(T)$ and dR/dT , where the signature of the CDW is absent at high pressure, in sharp contrast to the ambient pressure data for the same flake (S55) (see Figs. 4(b) and 4(c)). In addition, the residual resistance values at 28.7 kbar and 39.9 kbar are comparable, but noticeably lower than that at ambient pressure (inset of Fig. 4(b)). This is because at 28.7 kbar and 39.9 kbar, the elimination of the CDW state implies the absence of the CDW-induced Fermi surface gapping, giving rise to a smaller resistance.

Further evidence for the removal of the CDW state at high pressure is provided by the absence of the anomalous Hall effect. Our ρ_{xy} data at ambient and high pressure strongly resembles the data reported by Yu *et al.* [17]: the characteristic ‘S shape’ line in the low-field region at ambient pressure attributable to AHE is also detected. At 28.7 kbar and 39.9 kbar, the curvature of $\rho_{xy}(B)$ varies more slowly, which can instead be described with a two-band model. Following Yu *et al.*, the disappearance of the AHE is tied to the removal of the CDW state.

We proceed to the measurement of the critical current under pressure. Figure 4(g) shows the V - I curves at selected temperatures at 28.7 kbar. Following the same procedure, we extract $I_{c,sf}(T)/I_{c,sf}(0)$ from dV/dI (see Fig. 4(h)), allowing a glimpse of the superconducting gap in CsV_3Sb_5 without the accompanying CDW order. At 28.7 kbar, $I_{c,sf}(T)/I_{c,sf}(0)$ can again be described by Eqns. (2) and (3), indicating an *s*-wave gap (Fig. 4(i)). At 39.9 kbar, which is ~ 1.6 to 2 times higher than the critical pressure at which T_{CDW} extrapolates to zero, we again obtain results consistent with an *s*-wave gap (see Figs. 4(j)-(l)). Note, however, the complicated structure in dV/dI at 39.9 kbar, and the existence of a sharp dip in

dV/dI beyond I_c . This can be caused by inhomogeneity, or the existence of another gap. Indeed, the analysis of the dip results in a gap-like temperature dependence with a *s*-wave symmetry (see Supporting Information S2). We tentatively remark that a second superconducting gap is possible in CsV_3Sb_5 . Nevertheless, these results unambiguously show that the CDW state does not modify the symmetry of the superconducting gap. This is in sharp contrast to the sister compound RbV_3Sb_5 , in which μSR detects a transition from a nodal to a nodeless gap when the CDW state is suppressed by pressure [47].

One aspect that is affected by the CDW order in CsV_3Sb_5 is the coupling strength, as benchmarked by the dimensionless ratio $2\Delta/k_B T_c$. The superconducting gap is 1.16 meV and 0.73 meV at 28.7 kbar and 39.9 kbar, respectively. These gap values gives $2\Delta/k_B T_c$ of 5.20 and 4.66, both smaller than the smallest value 5.30 at ambient pressure (Fig. 3(g)). Nevertheless, $2\Delta/k_B T_c$ are all higher than the BCS weak-coupling limit over the pressure range we investigated. Thus, superconductivity in CsV_3Sb_5 is strong-coupling, but the coupling strength appears to be sensitive to pressure.

The observed conventional *s*-wave superconductivity is consistent with other CDW systems [48–50], and the evolution of the coupling strength is reminiscent of $(\text{Sr,Ca})_3\text{Rh}_4\text{Sn}_{13}$, in which the coupling strength is progressively enhanced towards the structural/CDW quantum critical point [49]. The enhancement of the coupling strength in $(\text{Sr,Ca})_3\text{Rh}_4\text{Sn}_{13}$ has been traced to the softening of a phonon mode associated with the second-order structural transition [51]. Recently, phonon softening has also been reported in $\text{Lu}(\text{Pt}_{1-x}\text{Pd}_x)_2\text{In}$, another superconducting system with a CDW transition tunable by x [52]. In CsV_3Sb_5 , the suppression of the CDW state may result in a quantum critical point. On approaching the quantum critical point from either side, part of the phonon spectrum would gradually be softened, leading to an enhanced $2\Delta/k_B T_c$. This scenario appears to explain our observation, as both 28.7 kbar and 39.9 kbar are beyond the CDW region and $2\Delta/k_B T_c$ shows a clear decreasing trend as the system moves away from the CDW phase. However, detailed studies are still needed to examine how $2\Delta/k_B T_c$ varies within the CDW phase. Recent first-principles density-functional theory calculations indeed reveal the softening of phonon modes around the L point of the Brillouin zone upon approaching the CDW phase from high pressure [53], lending support to our experimental results.

METHODS

Crystal growths. Single crystals of CsV_3Sb_5 were synthesized from Cs (ingot, 99.95 %), V (powder, 99.9 %) and Sb (shot, 99.9999 %) using self-flux method similar to Refs. [1, 2]. The cooling rate of the final segment of the growth profile was adjusted to prepare samples with varying RRR values. For example, the best sample comes from the growth where the final segment was

cooling from 900°C to room temperature at 0.5°C/hr, while for the sample with $\text{RRR} < 30$, the corresponding cooling rate was 2°C/hr.

High pressure. We adopt the concept of “device integrated diamond anvil cell” developed by us for high-pressure studies [54, 55]. Our anvils were patterned with microelectrodes by photo-lithography and physical vapour deposition coating. Thin flakes of CsV_3Sb_5 were exfoliated from single crystals and then transferred onto the patterned electrodes. A thin layer of h-BN was added onto the thin flakes for encapsulation. The thickness of the thin flakes was determined by a dual-beam focused ion beam system (Scios 2 DualBeam by Thermo Scientific) prior to pressurization. High-purity glycerine 99.5% was used as the pressure transmitting medium. The pressure achieved was determined by ruby fluorescence at room temperature [56].

Measurements. Electrical resistivity was measured by a standard four-terminal configuration in Physical Property Measurement System by Quantum Design and a dilution refrigerator by Bluefors. Dupont 6838 silver paste was used for making the electrical contacts on bulk crystals, while a set of patterned electrodes was used to form a tight contact with thin flakes exfoliated from the bulk crystals [54, 55]. V - I curves were measured by a Keithley 2182A nanovoltmeter together with a Keithley 6221 current source in the pulsed delta mode. The duration of the pulsed current was 11 ms, and the pulse repetition time was 1 s.

ASSOCIATED CONTENT

Supporting Information

The Supporting Information is available free of charge via the internet at <http://pubs.acs.org>. Figures S1 and S2 display additional $\rho(T)$ data and Fig. S3 shows the RRR dependence of T_{CDW} . Figure S4 is the analysis of the dip feature in dV/dI at 39.9 kbar. Table S1 displays the comparison of the superconducting gap magnitude with previous studies.

AUTHOR INFORMATION

Corresponding Authors

*Kwing To Lai. E-mail: ktlai@phy.cuhk.edu.hk

†Swee K. Goh. E-mail: skgoh@cuhk.edu.hk

Author Contributions

S.K.G. proposed and supervised the project. W.Z. coordinated the experimental efforts. W.Z., X.L., L.W. and W.W. conducted measurements, C.W.T., S.T.L. and K.T.L. prepared single crystals of CsV_3Sb_5 . J.X. provided assistance with pressure cells. X.Z., Y.Z. and S.W. provided h-BN. J.L.T. provided theoretical support. W.Z., Z.W. and S.K.G. performed data analysis. W.Z., K.T.L. and S.K.G. wrote the manuscript with

input from all authors.

Notes

The authors declare no competing financial interest.

Data availability

All the data that support the findings of this paper are available from the corresponding authors upon reasonable request.

ACKNOWLEDGMENTS

The authors acknowledge insightful comments from Yajian Hu and Chongze Wang. This work was supported by Research Grants Council of Hong Kong (CUHK 14301020, CUHK 14300722, A-CUHK402/19), CUHK Direct Grant (4053461, 4053408, 4053528, 4053463), the National Natural Science Foundation of China (12104384, 12174175) and the Shenzhen Basic Research Fund (JCYJ20190809173213150).

REFERENCES

- [1] B. R. Ortiz, L. C. Gomes, J. R. Morey, M. Winiarski, M. Bordelon, J. S. Mangum, I. W. H. Oswald, J. A. Rodriguez-Rivera, J. R. Neilson, S. D. Wilson, E. Ertekin, T. M. McQueen, and E. S. Toberer, “New kagome prototype materials: discovery of KV_3Sb_5 , RbV_3Sb_5 , and CsV_3Sb_5 ,” *Phys. Rev. Mater.* **3**, 094407 (2019).
- [2] B. R. Ortiz, S. M. L. Teicher, Y. Hu, J. L. Zuo, P. M. Sarte, E. C. Schueller, A. M. M. Abeykoon, M. J. Krogstad, S. Rosenkranz, R. Osborn, R. Seshadri, L. Balents, J. He, and S. D. Wilson, “ CsV_3Sb_5 : A \mathbb{Z}_2 topological kagome metal with a superconducting ground state,” *Phys. Rev. Lett.* **125**, 247002 (2020).
- [3] F. Du, S. Luo, B. R. Ortiz, Y. Chen, W. Duan, D. Zhang, X. Lu, S. D. Wilson, Y. Song, and H. Yuan, “Pressure-induced double superconducting domes and charge instability in the kagome metal KV_3Sb_5 ,” *Phys. Rev. B* **103**, L220504 (2021).
- [4] K. Y. Chen, N. N. Wang, Q. W. Yin, Y. H. Gu, K. Jiang, Z. J. Tu, C. S. Gong, Y. Uwatoko, J. P. Sun, H. C. Lei, J. P. Hu, and J.-G. Cheng, “Double superconducting dome and triple enhancement of T_c in the kagome superconductor CsV_3Sb_5 under high pressure,” *Phys. Rev. Lett.* **126**, 247001 (2021).
- [5] H. Li, T. T. Zhang, T. Yilmaz, Y. Y. Pai, C. E. Marvinney, A. Said, Q. W. Yin, C. S. Gong, Z. J. Tu, E. Vescovo, C. S. Nelson, R. G. Moore, S. Murakami, H. C. Lei, H. N. Lee, B. J. Lawrie, and H. Miao, “Observation of unconventional charge density wave without acoustic phonon anomaly in kagome superconductors AV_3Sb_5 ($A = \text{Rb}, \text{Cs}$),” *Phys. Rev. X* **11**, 031050 (2021).
- [6] Z. Liang, X. Hou, F. Zhang, W. Ma, P. Wu, Z. Zhang, F. Yu, J.-J. Ying, K. Jiang, L. Shan, Z. Wang, and X.-H. Chen, “Three-dimensional charge density wave and surface-dependent vortex-core states in a kagome superconductor CsV_3Sb_5 ,” *Phys. Rev. X* **11**, 031026 (2021).

- [7] H. Zhao, H. Li, B. R. Ortiz, S. M. L. Teicher, T. Park, M. Ye, Z. Wang, L. Balents, S. D. Wilson, and I. Zeljkovic, “Cascade of correlated electron states in the kagome superconductor CsV_3Sb_5 ,” *Nature* **599**, 216 (2021).
- [8] Z. Liu, N. Zhao, Q. Yin, C. Gong, Z. Tu, M. Li, W. Song, Z. Liu, D. Shen, Y. Huang, K. Liu, H. Lei, and S. Wang, “Charge-density-wave-induced bands renormalization and energy gaps in a kagome superconductor RbV_3Sb_5 ,” *Phys. Rev. X* **11**, 041010 (2021).
- [9] Y. Hu, S. M. L. Teicher, B. R. Ortiz, Y. Luo, S. Peng, L. Huai, J. Z. Ma, N. C. Plumb, S. D. Wilson, J. F. He, and M. Shi, “Charge-order-assisted topological surface states and flat bands in the kagome superconductor CsV_3Sb_5 ,” *Sci. Bull.* **67**, 495 (2022).
- [10] E. Uykur, B. R. Ortiz, S. D. Wilson, M. Dressel, and A. A. Tsirlin, “Optical detection of charge-density-wave instability in the non-magnetic kagome metal KV_3Sb_5 ,” *npj Quantum Mater.* **7**, 16 (2022).
- [11] X. Zhou, Y. Li, X. Fan, J. Hao, Y. Dai, Z. Wang, Y. Yao, and H.-H. Wen, “Origin of charge density wave in the kagome metal CsV_3Sb_5 as revealed by optical spectroscopy,” *Phys. Rev. B* **104**, L041101 (2021).
- [12] Y.-X. Jiang, J.-X. Yin, M. M. Denner, N. Shumiya, B. R. Ortiz, G. Xu, Z. Guguchia, J. He, M. S. Hossain, X. Liu, J. Ruff, L. Kautzsch, S. S. Zhang, G. Chang, I. Belopolski, Q. Zhang, T. A. Cochran, D. Multer, M. Litskevich, Z.-J. Cheng, X. P. Yang, Z. Wang, R. Thomale, T. Neupert, S. D. Wilson, and M. Z. Hasan, “Unconventional chiral charge order in kagome superconductor KV_3Sb_5 ,” *Nat. Mater.* **20**, 1353 (2021).
- [13] M. Kang, S. Fang, J.-K. Kim, B. R. Ortiz, S. H. Ryu, J. Kim, J. Yoo, G. Sangiovanni, D. Di Sante, B.-G. Park, C. Jozwiak, A. Bostwick, E. Rotenberg, E. Kaxiras, S. D. Wilson, J.-H. Park, and R. Comin, “Twofold van Hove singularity and origin of charge order in topological kagome superconductor CsV_3Sb_5 ,” *Nat. Phys.* **18**, 301 (2022).
- [14] M. Kang, S. Fang, J. Yoo, B. R. Ortiz, Y. Oey, S. H. Ryu, J. Kim, C. Jozwiak, A. Bostwick, E. Rotenberg, E. Kaxiras, J. Checkelsky, S. D. Wilson, J.-H. Park, and R. Comin, “Microscopic structure of three-dimensional charge order in kagome superconductor AV_3Sb_5 and its tunability,” 2022, 2202.01902, arXiv, <https://arxiv.org/abs/2202.01902> (Accessed September 18th, 2022).
- [15] S. Wu, B. R. Ortiz, H. Tan, S. D. Wilson, B. Yan, T. Birol, and G. Blumberg, “Charge density wave order in the kagome metal AV_3Sb_5 ($A = \text{Cs}, \text{Rb}, \text{K}$),” *Phys. Rev. B* **105**, 155106 (2022).
- [16] R. Lou, A. Fedorov, Q. Yin, A. Kuibarov, Z. Tu, C. Gong, E. F. Schwier, B. Büchner, H. Lei, and S. Borisenko, “Charge-density-wave-induced peak-dip-hump structure and the multiband superconductivity in a kagome superconductor CsV_3Sb_5 ,” *Phys. Rev. Lett.* **128**, 036402 (2022).
- [17] F. H. Yu, T. Wu, Z. Y. Wang, B. Lei, W. Z. Zhuo, J. J. Ying, and X. H. Chen, “Concurrence of anomalous Hall effect and charge density wave in a superconducting topological kagome metal,” *Phys. Rev. B* **104**, L041103 (2021).
- [18] S.-Y. Yang, Y. Wang, B. R. Ortiz, D. Liu, J. Gayles, E. Derunova, R. Gonzalez-Hernandez, L. Šmejkal, Y. Chen, S. S. P. Parkin, S. D. Wilson, E. S. Toberer, T. McQueen, and M. N. Ali, “Giant, unconventional anomalous Hall effect in the metallic frustrated magnet candidate, KV_3Sb_5 ,” *Sci. Adv.* **6**, eabb6003 (2020).
- [19] F. Yu, D. Ma, W. Zhuo, S. Liu, X. Wen, B. Lei, J. Ying, and X. Chen, “Unusual competition of superconductivity and charge-density-wave state in a compressed topological kagome metal,” *Nat. Commun.* **12**, 3645 (2021).
- [20] J. Yu, Z. Xu, K. Xiao, Y. Yuan, Q. Yin, Z. Hu, C. Gong, Y. Guo, Z. Tu, P. Tang, et al., “Evolution of electronic structure in pristine and Rb-reconstructed surfaces of kagome metal RbV_3Sb_5 ,” *Nano Lett.* **22**, 918 (2022).
- [21] L. Yu, C. Wang, Y. Zhang, M. Sander, S. Ni, Z. Lu, S. Ma, Z. Wang, Z. Zhao, H. Chen, K. Jiang, Y. Zhang, H. Yang, F. Zhou, X. Dong, S. L. Johnson, M. J. Graf, J. Hu, H.-J. Gao, and Z. Zhao, “Evidence of a hidden flux phase in the topological kagome metal CsV_3Sb_5 ,” 2021, 2107.10714, arXiv, <https://arxiv.org/abs/2107.10714> (Accessed September 18th, 2022).
- [22] Y. Hu, S. Yamane, G. Mattoni, K. Yada, K. Obata, Y. Li, Y. Yao, Z. Wang, J. Wang, C. Farhang, et al., “Time-reversal symmetry breaking in charge density wave of CsV_3Sb_5 detected by polar kerr effect,” 2022, 2208.08036, arXiv, <https://arxiv.org/abs/2208.08036> (Accessed September 18th, 2022).
- [23] X. Feng, K. Jiang, Z. Wang, and J. Hu, “Chiral flux phase in the kagome superconductor AV_3Sb_5 ,” *Sci. Bull.* **66**, 1384 (2021).
- [24] H.-S. Xu, Y.-J. Yan, R. Yin, W. Xia, S. Fang, Z. Chen, Y. Li, W. Yang, Y. Guo, and D.-L. Feng, “Multiband superconductivity with sign-preserving order parameter in kagome superconductor CsV_3Sb_5 ,” *Phys. Rev. Lett.* **127**, 187004 (2021).
- [25] H. Chen, H. Yang, B. Hu, Z. Zhao, J. Yuan, Y. Xing, G. Qian, Z. Huang, G. Li, Y. Ye, et al., “Roton pair density wave in a strong-coupling kagome superconductor,” *Nature* **599**, 222 (2021).
- [26] C. Zhao, L. Wang, W. Xia, Q. Yin, J. Ni, Y. Huang, C. Tu, Z. Tao, Z. Tu, C. Gong, et al., “Nodal superconductivity and superconducting domes in the topological kagome metal CsV_3Sb_5 ,” 2021, 2102.08356, arXiv, <https://arxiv.org/abs/2102.08356> (Accessed September 18th, 2022).
- [27] R. Gupta, D. Das, C. H. Mielke III, Z. Guguchia, T. Shiroka, C. Baines, M. Bartkowiak, H. Luetkens, R. Khasanov, Q. Yin, et al., “Microscopic evidence for anisotropic multigap superconductivity in the CsV_3Sb_5 kagome superconductor,” *npj Quant. Mater.* **7**, 49 (2022).
- [28] R. Gupta, D. Das, C. Mielke, E. T. Ritz, F. Hotz, Q. Yin, Z. Tu, C. Gong, H. Lei, T. Birol, R. M. Fernandes, Z. Guguchia, H. Luetkens, and R. Khasanov, “Two types of charge order with distinct interplay with superconductivity in the kagome material CsV_3Sb_5 ,” *Commun. Phys.* **5**, 232 (2022).
- [29] W. Duan, Z. Nie, S. Luo, F. Yu, B. R. Ortiz, L. Yin, H. Su, F. Du, A. Wang, Y. Chen, et al., “Nodeless superconductivity in the kagome metal CsV_3Sb_5 ,” *Sci. China: Phys. Mech. Astron.* **64**, 107462 (2021).
- [30] Z. Shan, P. K. Biswas, S. K. Ghosh, T. Tula, A. D. Hillier, D. Adroja, S. Cottrell, G.-H. Cao, Y. Liu, X. Xu, Y. Song, H. Yuan, and M. Smidman, “Muon spin relaxation study of the layered kagome superconductor CsV_3Sb_5 ,” *Phys. Rev. Research* **4**, 033145 (2022).

- [31] M. Roppongi, K. Ishihara, Y. Tanaka, K. Ogawa, K. Okada, S. Liu, K. Mukasa, Y. Mizukami, Y. Uwatoko, R. Grasset, et al., “Bulk evidence of anisotropic s -wave pairing with no sign change in the kagome superconductor CsV_3Sb_5 ,” 2022, 2206.02580, arXiv, <https://arxiv.org/abs/2206.02580> (Accessed September 18th, 2022).
- [32] C. Mu, Q. Yin, Z. Tu, C. Gong, H. Lei, Z. Li, and J. Luo, “ S -wave superconductivity in kagome metal CsV_3Sb_5 revealed by $^{121/123}\text{Sb}$ NQR and ^{51}V NMR measurements,” *Chin. Phys. Lett.* **38**, 077402 (2021).
- [33] E. F. Talantsev and J. L. Tallon, “Universal self-field critical current for thin-film superconductors,” *Nat. Commun.* **6**, 7820 (2015).
- [34] E. F. Talantsev, W. P. Crump, and J. L. Tallon, “Universal scaling of the self-field critical current in superconductors: from sub-nanometre to millimetre size,” *Sci. Rep.* **7**, 10010 (2017).
- [35] X. Liu, W. Zhang, K. T. Lai, K. Moriyama, J. L. Tallon, K. Yoshimura, and S. K. Goh, “Peak in the critical current density in $(\text{Ca}_x\text{Sr}_{1-x})_3\text{Rh}_4\text{Sn}_{13}$ tuned towards the structural quantum critical point,” *Phys. Rev. B* **105**, 214524 (2022).
- [36] S. Seo, E. Park, E. Bauer, F. Ronning, J. Kim, J.-H. Shim, J. Thompson, and T. Park, “Controlling superconductivity by tunable quantum critical points,” *Nat. Commun.* **6**, 6433 (2015).
- [37] D. V. Semenov, I. A. Troyan, A. V. Sadakov, D. Zhou, M. Galasso, A. G. Kvashnin, I. A. Kruglov, A. A. Bykov, K. Y. Terent’ev, A. V. Cherepahin, O. A. Sobolevskiy, K. S. Pervakov, A. Y. Seregin, T. Helm, T. Förster, A. D. Grockowiak, S. W. Tozer, Y. Nakamoto, K. Shimizu, V. M. Pudalov, I. S. Lyubutin, and A. R. Oganov, “Effect of magnetic impurities on superconductivity in LaH_{10} ,” *Adv. Mater.* **34**, 2204038 (2022).
- [38] P. W. Anderson, “Theory of dirty superconductors,” *J. of Phys. and Chem. of Solids* **11**, 26 (1959).
- [39] P. J. Hirschfeld, “Using gap symmetry and structure to reveal the pairing mechanism in Fe-based superconductors,” *C. R. Phys.* **17**, 197 (2016).
- [40] A. Mackenzie, R. Haselwimmer, A. Tyler, G. Lonzarich, Y. Mori, S. Nishizaki, and Y. Maeno, “Extremely strong dependence of superconductivity on disorder in Sr_2RuO_4 ,” *Phys. Rev. Lett.* **80**, 161 (1998).
- [41] J. Chen, K. Semeniuk, Z. Feng, P. Reiss, P. Brown, Y. Zou, P. W. Logg, G. I. Lampronti, and F. M. Grosche, “Unconventional superconductivity in the layered iron germanide YFe_2Ge_2 ,” *Phys. Rev. Lett.* **116**, 127001 (2016).
- [42] Y. Mizukami, M. Konczykowski, Y. Kawamoto, S. Kurata, S. Kasahara, K. Hashimoto, V. Mishra, A. Kreisler, Y. Wang, P. Hirschfeld, et al., “Disorder-induced topological change of the superconducting gap structure in iron pnictides,” *Nat. Commun.* **5**, 5657 (2014).
- [43] R. Prozorov, M. Kończykowski, M. A. Tanatar, A. Thaler, S. L. Bud’ko, P. C. Canfield, V. Mishra, and P. Hirschfeld, “Effect of electron irradiation on superconductivity in single crystals of $\text{Ba}(\text{Fe}_{1-x}\text{Ru}_x)_2\text{As}_2$ ($x=0.24$),” *Phys. Rev. X* **4**, 041032 (2014).
- [44] L. Nie, K. Sun, W. Ma, D. Song, L. Zheng, Z. Liang, P. Wu, F. Yu, J. Li, M. Shan, et al., “Charge-density-wave-driven electronic nematicity in a kagome superconductor,” *Nature* **604**, 59 (2022).
- [45] W. Zhang, L. Wang, C. W. Tsang, X. Liu, J. Xie, W. C. Yu, K. T. Lai, and S. K. Goh, “Emergence of large quantum oscillation frequencies in thin flakes of a kagome superconductor CsV_3Sb_5 ,” *Phys. Rev. B* **106**, 195103 (2022).
- [46] P.-G. De Gennes and P. A. Pincus, *Superconductivity of metals and alloys* (CRC Press, 2018).
- [47] Z. Guguchia, C. Mielke, D. Das, R. Gupta, J. X. Yin, H. Liu, Q. Yin, M. H. Christensen, Z. Tu, C. Gong, N. Shumiya, T. Gamsakhurdashvili, M. Elenker, P. Dai, A. Amato, Y. Shi, H. C. Lei, R. M. Fernandes, M. Z. Hasan, H. Luetkens, and R. Khasanov, “Tunable nodal kagome superconductivity in charge ordered RbV_3Sb_5 ,” 2022, 2202.07713, arXiv, <https://arxiv.org/abs/2202.07713> (Accessed September 18th, 2022).
- [48] S. K. Goh, D. A. Tompsett, P. J. Saines, H. C. Chang, T. Matsumoto, M. Imai, K. Yoshimura, and F. M. Grosche, “Ambient Pressure Structural Quantum Critical Point in the Phase Diagram of $(\text{Ca}_x\text{Sr}_{1-x})_3\text{Rh}_4\text{Sn}_{13}$,” *Phys. Rev. Lett.* **114**, 097002 (2015).
- [49] W. C. Yu, Y. W. Cheung, P. J. Saines, M. Imai, T. Matsumoto, C. Michioka, K. Yoshimura, and S. K. Goh, “Strong Coupling Superconductivity in the Vicinity of the Structural Quantum Critical Point in $(\text{Ca}_x\text{Sr}_{1-x})_3\text{Rh}_4\text{Sn}_{13}$,” *Phys. Rev. Lett.* **115**, 207003 (2015).
- [50] T. Gruner, D. Jang, Z. Huesges, R. Cardoso-Gil, G. H. Fecher, M. M. Koza, O. Stockert, A. P. Mackenzie, M. Brando, and C. Geibel, “Charge density wave quantum critical point with strong enhancement of superconductivity,” *Nat. Phys.* **13**, 967 (2017).
- [51] Y. W. Cheung, Y. J. Hu, M. Imai, Y. Tanioku, H. Kanagawa, J. Murakawa, K. Moriyama, W. Zhang, K. T. Lai, K. Yoshimura, F. M. Grosche, K. Kaneko, S. Tsutsui, and S. K. Goh, “Evidence of a structural quantum critical point in $(\text{Ca}_x\text{Sr}_{1-x})_3\text{Rh}_4\text{Sn}_{13}$ from a lattice dynamics study,” *Phys. Rev. B* **98**, 161103 (2018).
- [52] T. Gruner, S. Lucas, C. Geibel, K. Kaneko, S. Tsutsui, K. Schmalzl, and O. Stockert, “Phonon softening in $\text{Lu}(\text{Pt}_{1-x}\text{Pd}_x)_2\text{In}$ close to a zero-temperature structural instability,” *Phys. Rev. B* **106**, 115142 (2022).
- [53] C. Wang, S. Liu, H. Jeon, Y. Jia, and J.-H. Cho, “Charge density wave and superconductivity in the kagome metal CsV_3Sb_5 around a pressure-induced quantum critical point,” *Phys. Rev. Mater.* **6**, 094801 (2022).
- [54] J. Xie, X. Liu, W. Zhang, S. M. Wong, X. Zhou, Y. Zhao, S. Wang, K. T. Lai, and S. K. Goh, “Fragile pressure-induced magnetism in FeSe superconductors with a thickness reduction,” *Nano Lett.* **21**, 9310 (2021).
- [55] C.-h. Ku, X. Liu, J. Xie, W. Zhang, S. T. Lam, Y. Chen, X. Zhou, Y. Zhao, S. Wang, S. Yang, et al., “Patterned diamond anvils prepared via laser writing for electrical transport measurements of thin quantum materials under pressure,” *Rev. Sci. Instrum.* **93**, 083912 (2022).
- [56] H. Mao, J.-A. Xu, and P. Bell, “Calibration of the ruby pressure gauge to 800 kbar under quasi-hydrostatic conditions,” *J. Geophys. Res. Solid Earth* **91**, 4673 (1986).